Final Report—September '97 to October '98

Development of an Active Twist Rotor for Wind-Tunnel Testing (NLPN 97–310)

Carlos E. S. Cesnik SangJoon Shin Nesbitt W. Hagood IV

Active Materials and Structures Laboratory
Massachusetts Institute of Technology
Department of Aeronautics and Astronautics
77 Massachusetts Avenue
Cambridge, Massachusetts 02139

SUMMARY

The development of the Active Twist Rotor prototype blade for hub vibration and noise reduction studies is presented in this report. Details of the modeling, design, and manufacturing are explored. The rotor blade is integrally twisted by direct strain actuation. This is accomplished by distributing embedded piezoelectric fiber composites along the span of the blade. The development of the analysis framework for this type of active blade is presented. The requirements for the prototype blade, along with the final design results are also presented. A detail discussion on the manufacturing aspects of the prototype blade is described. Experimental structural characteristics of the prototype blade compare well with design goals, and preliminary bench actuation tests show lower performance than originally predicted. Electrical difficulties with the actuators are also discussed. The presented prototype blade is leading to a complete fully articulated four-blade active twist rotor system for future wind tunnel tests.

INTRODUCTION

The technology of smart structures provides a new degree of design flexibility for individual blade control (IBC) of advanced composite helicopter rotor blades.[1-2] The key to the technology is the ability to allow the structure to sense and react in a desired fashion, with potential improvements in rotor blade performance, especially in the areas of structural vibration, acoustic signature, and aeroelastic stability.

The broad class of actuation approaches for helicopter IBC can be basically subdivided in two groups: actuated control surfaces at discrete locations along the blade,[3-9] and direct deformation (usually twist) of the blade structure.[10-17] The present work falls on the latter.

Recent analytical and experimental investigations have indicated that the active fiber composites embedded in composite rotor blade structures should be capable of meeting the performance requirements necessary for a useful individual blade control system.[12-17] The active fiber composite (AFC) actuator utilizes interdigitated electrode poling and piezoelectric fiber embedded in an epoxy matrix[18] as shown in Fig. 1. This combination results in a high performance piezoelectric actuator laminate with strength and conformability characteristics much greater than that of a conventional monolithic piezoceramic. Among the efforts in this area of direct deformation of the blade using AFC actuators is the collaborative program between Boeing Co. and MIT (sponsored by DARPA). This program has been addressing the different manufacturing issues of an integrally twisted blade using the AFC actuators. A single 1/6th Mach scale CH-47D model blade was constructed and hover tests were conducted, showing encouraging results.[17] Future design and manufacturing of a three-bladed 1/6th CH-47D rotor system is expected to happen for eventual Mach-scaled wind tunnel tests in air (where specific demonstrations of full-scale blade stresses will be possible).

NASA Langley Cooperative Agreement #NCC1-259

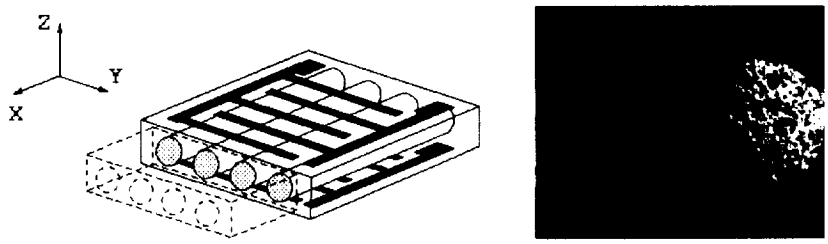

Figure 1. Active Fiber Composites (AFC) showing (a) mode of actuation along the fiber direction, and (b) SEM picture showing the piezoelectric fibers in a epoxy matrix.

In a complementary manner, a research program between NASA Langley/Army Research Laboratory and MIT has been established to investigate the specific issues related to the modeling and design of active twist rotor (ATR) systems, evaluate their effectiveness for IBC in forward flight, and the impact on vibration and noise reduction, as well as potential cyclic control of future active systems. As part of the ATR program, extensive wind tunnel test will support the proposed concept and will provide a first-of-a-kind experimental data for validation of the developed modeling approaches. The test will be accomplished using a 2.74-m diameter 4-bladed fully-articulated aeroelastically scaled wind tunnel model designed for testing in the heavy gas environment of the NASA Langley Transonic Dynamics Tunnel (TDT).[19] The Aeroelastic Rotor Experimental System (ARES), pictured in the TDT in Fig. 2, will be used to test the ATR model. The TDT utilizes a heavy gas test medium with a speed of sound approximately one half that of sea level standard air. This, along with the TDT's variable density test capability, permits full scale rotor tip Mach numbers, Froude numbers, and Lock numbers to be matched simultaneously at model scale. In particular, the reduced speed of sound in the heavy gas medium allows full-scale tip Mach numbers to be matched at lower rotational speeds and lower blade stresses.

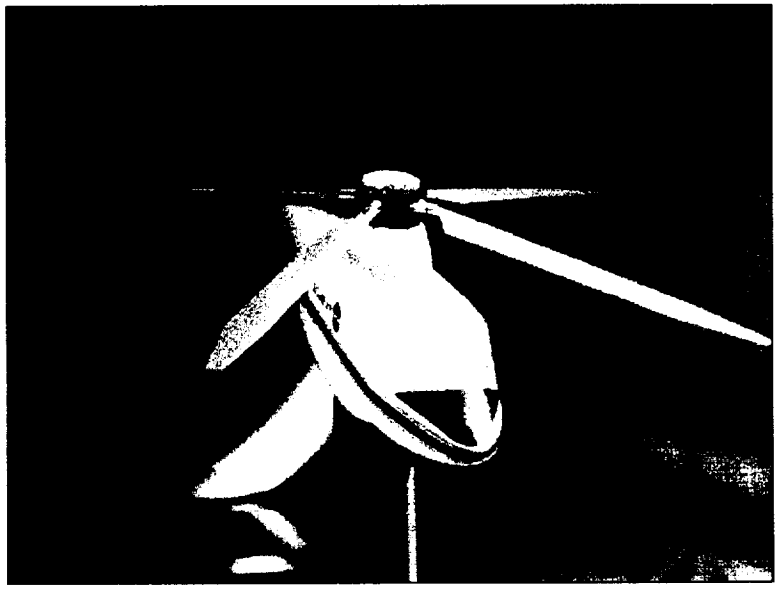

Figure 2. Aeroelastic Rotor Experimental System (ARES) 9 ft diameter rotor testbed in Langley Transonic Dynamics Tunnel (TDT).

A prototype ATR model rotor blade for such test system has been under investigation at MIT Active Materials and Structures Laboratory (AMSL). The prototype ATR blade is to be used for non-rotating bench tests and single blade spin tests to evaluate the baseline ATR design and construction methods. After completion of these tests, a set of four ATR model blades based on the prototype design will be constructed for wind tunnel testing. The objective of this paper is to present the methodology used to model and design this prototype blade, its manufacturing highlights, and bench test results.

ATR BLADE MODELING

Due to the lack of reliable analysis formulations to design an active helicopter blade cross section like the ATR concept, the authors have been working on creating a general framework for active rotor blade modeling. It builds on the state-of-the-art framework for passive blades presented in Ref. 20, and it is divided in three main components: (2-D) cross-sectional analysis, (1-D) beam analysis, and laminae stress recovery analysis (see Fig. 3).

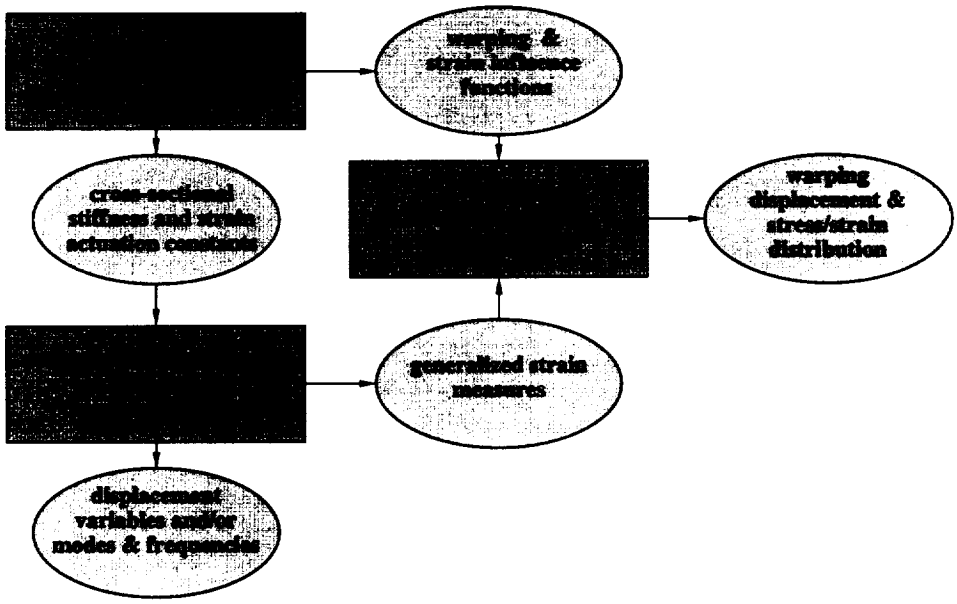

Figure 3. Three-dimensional framework for analyzing active rotor blades.

Cross-sectional Analysis

An analytic formulation for a two-cell thin-walled composite beam with integral anisotropic piezoelectric actuators is derived to design and analyze an active twist helicopter rotor blade. It is an asymptotically correct formulation stemming from shell theory.

The new asymptotical formulation to analyze multi-cell composite beams incorporating embedded piezoelectric plies distributed throughout the blade was developed and presented in details in Ref. 21. While restricted to thin-walled beams, it yields closed form solutions of the displacement field (which is derived and *not* assumed), and stiffness and actuation constants. The availability of correct closed form expressions was essential to determine design paradigms on this new type of blade, mainly concerning to the tradeoffs between torsional stiffness and twist actuation. These stiffness and actuation constants will then be used in a beam finite element discretization of the blade reference line.

Even though details of this formulation can be found in Ref. 21, the main results are reproduced below for completeness. Consider the blade idealization as presented in Fig. 4. With an assumed linear piezoelectric constitute relation and starting from a shell strain energy, the 2-D original electroelastic shell formulation is condensed to a 1-D beam problem. The displacement field is found to be:

$$\begin{aligned} v_1 &= u_1(x) - y(s)u_2'(x) - z(s)u_3'(x) + \\ &\quad + G(s)\phi'(x) + g_1(s)u_1'(x) + \\ &\quad + g_2(s)u_2''(x) + g_3(s)u_3''(x) + v_1^{(a)}(s) \\ v_2 &= u_2(x)\frac{dy}{ds} + u_3(x)\frac{dz}{ds} + \phi(x)r_n \\ v_3 &= u_2(x)\frac{dz}{ds} - u_3(x)\frac{dy}{ds} - \phi(x)r_n \end{aligned}$$

where the superscript *(a)* indicates that the component is function of the applied electric field (in this case of thin-walled cross sections, the actuation only influences the out-of-plane component of the displacement field). The functions $G(s)$ and $g_i(s)$ are the warping functions associated with torsion, extension, and two bending measures. Associated with this displacement field, the beam constitutive relation relating beam generalized forces (axial force, twist, and two bending moments, respectively) with beam generalized strains (axial strain, twist curvature, and two bending curvatures) and corresponding generalized actuation forces (function of the geometry, material distribution, and applied electric field) is obtained in the following form:

$$\begin{Bmatrix} F_1 \\ M_1 \\ M_2 \\ M_3 \end{Bmatrix} = \begin{bmatrix} K_{11} & K_{12} & K_{13} & K_{14} \\ K_{12} & K_{22} & K_{23} & K_{24} \\ K_{13} & K_{23} & K_{33} & K_{34} \\ K_{14} & K_{24} & K_{34} & K_{44} \end{bmatrix} \begin{Bmatrix} \gamma_{11} \\ \kappa_1 \\ \kappa_2 \\ \kappa_3 \end{Bmatrix} - \begin{Bmatrix} F_1^{(a)} \\ M_1^{(a)} \\ M_2^{(a)} \\ M_3^{(a)} \end{Bmatrix}$$

where $[K]$ is the stiffness matrix function of geometry and material distribution at the rotor cross section. From this formulation, all K_{ij} and the generalized actuation forces are given by closed form expressions.[21]

1-D Beam Analysis

The geometrically exact beam equations of Ref. 22 were extended to deal with distributed actuation. The original nonlinear formulation allows for small strain and finite rotations, and is cast in a mixed variational intrinsic form. The extension of that to incorporate embedded actuation effects was done by bringing the new constitutive relation previously described into the 1-D finite element formulation, and its implementation was performed on the aeroelastic hover solution described in Ref. 23. Again, details of that can be found in Ref. 21. The solution of the 1-D beam analysis provides blade displacement and generalized stress fields due to external loading and piezoelectric actuation, which are of interest in the analysis of static and dynamic deformations and aeroelastic stability.

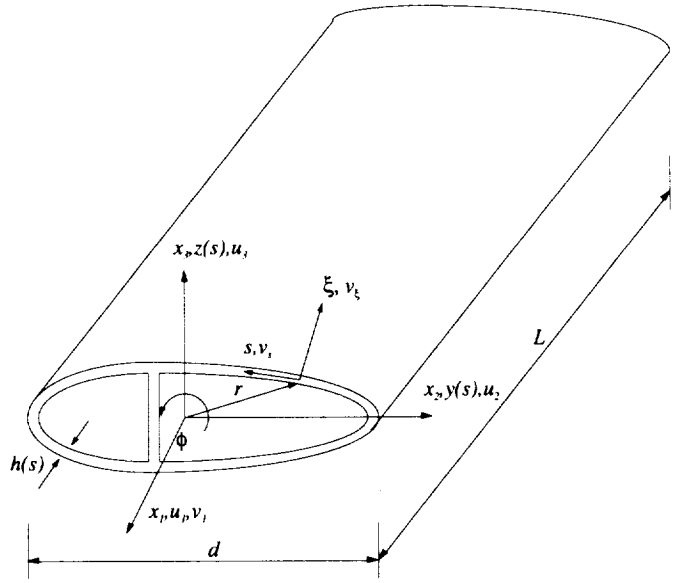

Figure 4. Two-cell thin-walled cross-section beam.

For the ATR program, however, hover loads were not enough to size the ATR blade. CAMRAD II comprehensive rotorcraft analysis[24] was used for preliminary study of the active twist rotor concept in forward flight. In particular, the vibration reduction capabilities of the ATR were studied using CAMRAD II because it offers a more detailed dynamic model and a free wake aerodynamic model. The integral twist actuation was modeled in CAMRAD II with a controlled external twisting couple applied at the blade root and blade tip. In this

manner, the strain produced by the AFCs could be simulated without modification of the finite element beam model available in the analysis. Details of such study are presented in Ref. 25.

Laminae Stress Recovery

For the final step, the stress within each composite layer is calculated with a combination of information from the cross-sectional analysis and the beam analysis. Flap and lead-lag bending, and torsion loads at discrete blade stations for forward flight can be combined with the cross sectional properties of the blade and generalized strains at the blade reference line can be directly calculated. These are then transformed to the shell strains in the cross-sectional wall reference frame. Finally, according to classical lamination plate theory, the mid-plane generalized strains can be converted to local strains at the k^{th} ply (with proper rotation so plane stresses can be calculated in material directions). Results from this last step are used to support the strength design of the active blade.

ATR BLADE DESIGN

Aeroelastic design of the active twist blade was accomplished within the framework described above. The basic requirements for the ATR prototype blade come from an existing passive blade used by NASA LaRC. The baseline (passive) system has been well studied and characterized along the years, and is representative of a typical production helicopter.[25] The new ATR blade is designed based on the external dimensions and aerodynamic properties of the existing baseline blade. Table 1 summarizes the general dimension and shape characteristics, and Table 2 presents the main structural characteristics of the baseline blade, as well as the result characteristics of the ATR prototype blade design. Finally, regarding actuation properties, the target was to provide an actuation level of approximately ±2° at the tip. This level of actuation authority should be sufficient to experimentally investigate a wide range of IBC active twist applications.[25]

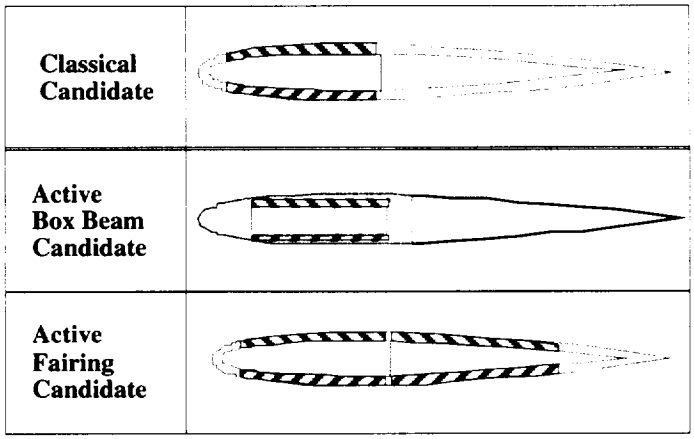

Figure 5. Different concepts of ATR blade candidates considered during the design studies (shaded areas indicate regions with AFC).

Different design studies including different cross-sectional actuation concepts were conducted to maximize actuation performance while satisfying stiffness, strength, and manufacturability constraints. A detailed study of the implications of distributing the torsional stiffness at different cross section members and the importance of having a multi-cell active cross-section analysis capability is presented in Ref. 26. A sample of three different concepts considered for the ATR blade is presented in Fig. 5. Also, forward flight loads were evaluated for each of the cases using CAMRAD II, and a sample result for the final design is presented in Fig. 6.

Table 1. General properties of the existing baseline rotor blade

Rotor type	Fully articulated
Number of blades, b	4
Blade chord, c	10.77 cm
Blade radius, R	1.4 m
Solidity, $bc/\pi R$	0.0982
Lock number	4.55
Airfoil shape	NACA 0012
Blade pretwist	–10° (linear from 0R to tip)
Hinge offset	7.62 cm
Root cutout	31.75 cm
Pitch axis	25% chord
Elastic axis	25% chord
Center of gravity	25% chord
Operational speed	687.5 rpm
Rotor overspeed	756 rpm

Table 2. Main characteristics of the ATR final design and the passive baseline blades

	Final Design	**Requirement (Baseline)**	**% Difference**
Mass per unit span (kg/m)	0.6960	0.6959	+0.01
x_{CG}/c	24.9 %	25%	–0.4
x_{TA}/c	30.8 %	25%	+23.2
K_{11} (axial) (N)	$1.637\ 10^{6}$	$2.0\ 10^{6}$	–18.2
K_{22} (torsional) (N-m^2)	$3.622\ 10^{1}$	$4.8468\ 10^{1}$	–25.3
K_{33} (flap bending) (N-m^2)	$4.023\ 10^{1}$	$4.3306\ 10^{1}$	–7.1
K_{44} (lead-lag) (N-m^2)	$1.094\ 10^{3}$	$7.0264\ 10^{3}$	–84.4
Lock No.	4.55	4.55	0.0
Section torsional inertia (kg-m^2/m)	$3.307\ 10^{-4}$	$3.1739\ 10^{-4}$	+4.2
1st torsion frequency @ 687.5 rpm	7.38/rev	7.37/rev	+0.1
Twist actuation @ 0 RPM (peak-to-peak, °/m)	4.52°	4°	+13.0
Maximum strain at the worst loading condition (@AFC) (μstrain)			
(1) Fiber direction	2,730		
(2) Transverse direction	2,730		
(3) Shear direction	5,170		

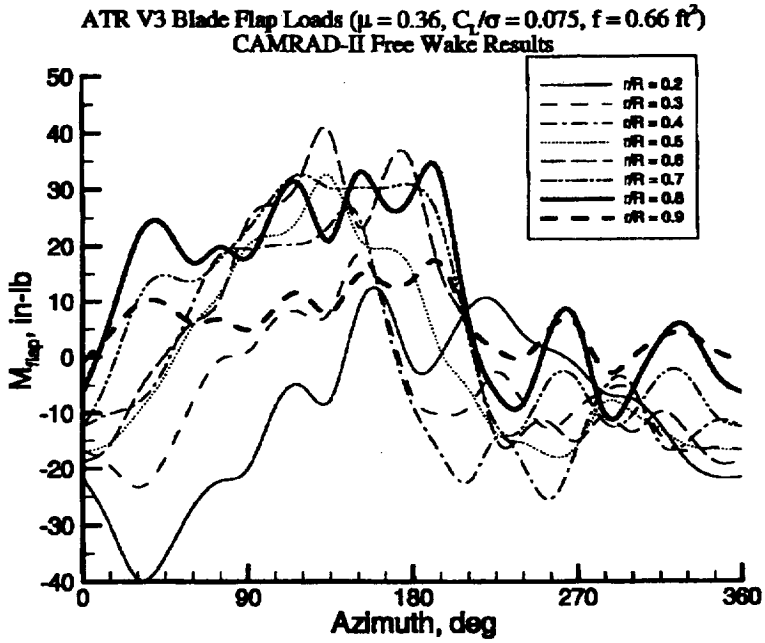

Figure 6. CAMRAD II forward flight loads prediction (flapwise blade loads for trimmed flight).

The chosen concept and converged structural design of the prototype Active Twist Rotor model blade is shown in Figs. 7 and 8. The final concept employs a total of 24 AFC packs placed on the front spar only, and distributed in 6 stations along the radius. Even though not the highest actuation authority concept, the chosen one satisfies all the requirements and provide a lower cost option (where most of the cost comes from the AFC packs). The AFC laminae are embedded in the blade structure at alternating ±45° orientation angles that maximize the twist actuation capabilities of the active plies. With an even number of AFC plies, it is also possible to keep the passive structure of the rotor blade virtually elastically uncoupled. This allows independent actuation of blade torsional motion with practically no bending or axial actuation. The ATR prototype blade was originally expected to achieve static twist actuation amplitudes of between 2.0° to 2.5°, and hovering flight dynamic twist actuation amplitudes of 2.0° to 4.0° (based on CAMRAD II and PETRA simulations[25]).

Structural integrity of the new blade design was evaluated based on the worst loading conditions, which are expected to occur within the rotor system operating envelope. In this design, forward flight with the maximum speed is selected as the loading criterion. Then, the largest magnitudes of the aerodynamic loads are extracted and combined with the centrifugal loads in order to give the worst loading values and a safety factor of 1.5 is used. The developed design tool is used to convert the 1-D global beam loading into the stress/strain existing in constituent composite plies within the skin lay-up. By adopting maximum strain as the static failure criterion, the structural strength is confirmed.

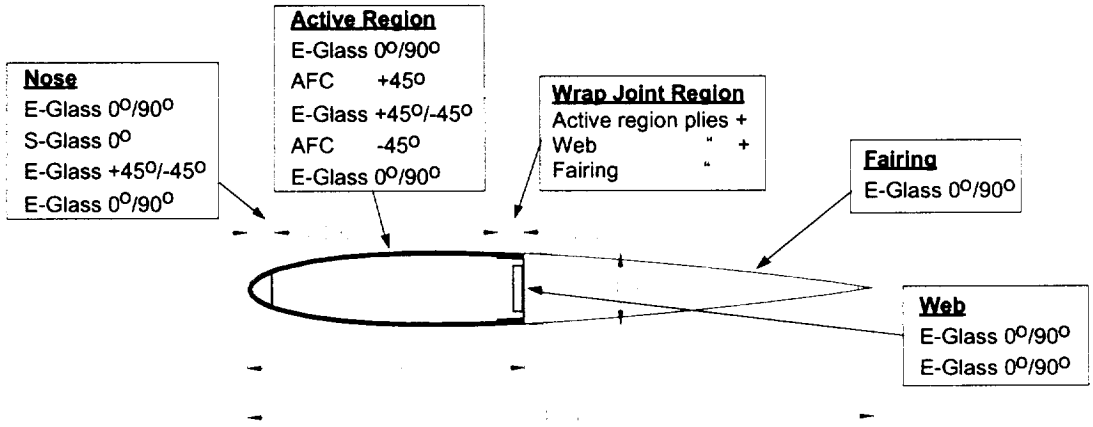

Figure 7. Schematic diagram of the final ATR blade section design. Dimensions are in inches.

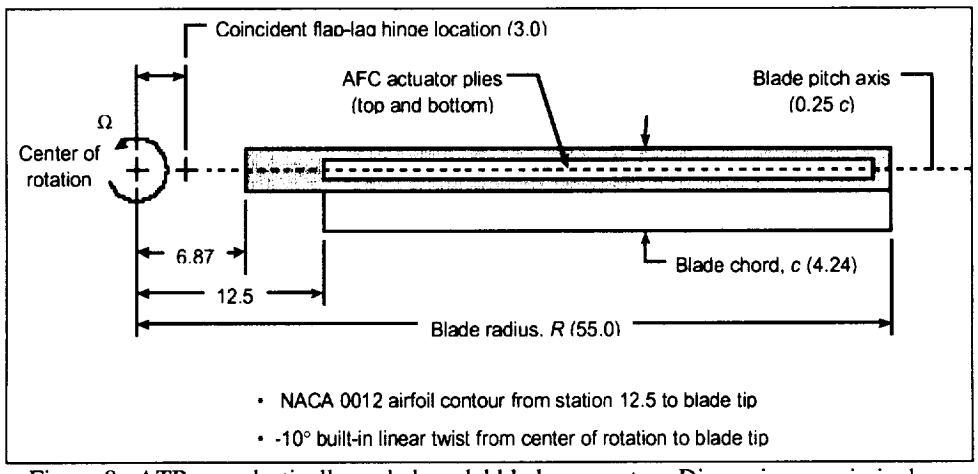

Figure 8. ATR aeroelastically scaled model blade geometry. Dimensions are in inches.

ATR PROTOTYPE MANUFACTURING

The prototype blade was manufactured according to the final design described above. The aluminum blade mold used for the original baseline blade manufacturing was used again for this prototype. Also, besides the details described above, there were some additional needs on different miscellaneous elements.

Miscellaneous Items

Among the different elements that needed special attention during this phase, one of special importance is the blade root, which was totally modified from the original metal block attachment of the baseline blade. The concept adopted for this blade uses an integral graphite/epoxy construction in the exact external airfoil shape, with a small Rohacell foam core to provide the back pressure during cure. A total of 80 plies of IM7 unidirectional graphite/epoxy were cut and laid-up to form the $[0°, +45°, -45°, 90°]_{10}$ symmetric laminate about the foam core. This was chosen in order to provide enough strength for tensile, bending and torsional loads. Also, for continuity of the outboard lay-up, the root is wrapped around by the continuum skin E-Glass plies of the outboard constant cross-section. Fig. 9 shows the graphite part of the root prior to cure. Finally, three bolts in tandem do the mounting of the blade root with the hub attachment. The corresponding holes that go through the root block are drilled using a diamond drill bit after the root stack is cured.

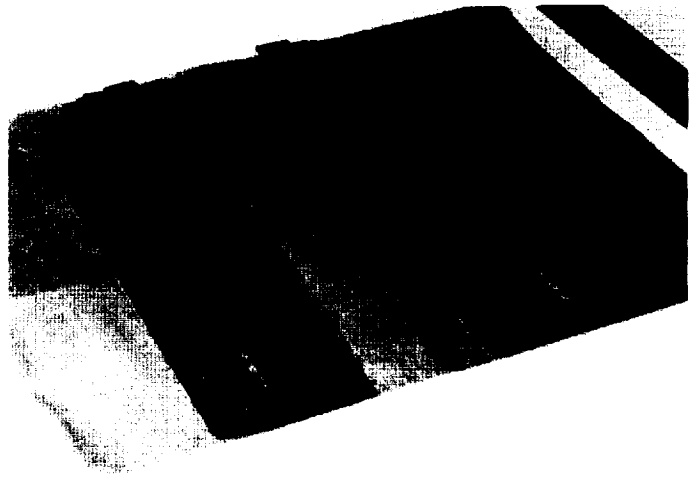
Figure 9. Detail of the blade root construction

Regarding the AFC packs used for this prototype blade, similar design and manufacturing procedures adopted for the Boeing/MIT CH-47D integral actuated blade[17] were used. The new blade geometry, however, required new pack dimensions and minor modifications on the gap between the AFC packs and the location of the solder flaps. The final geometry of the AFC packs is presented in Fig. 10. The manufacturing of all 24 individual AFC packs were performed by Continuum Control Corp., Cambridge, Massachusetts, according to the specifications. Before using the packs on the composite construction, each of them were individually tested and their actuation and capacitance characterized at two different cycles: 3,000 V_{pp}/600 V_{DC} ("representative cycle") and 4,000 V_{pp}/1,200 V_{DC} ("extended cycle") for 1 and 10 Hz. The average free strain for the extended cycle was 1278 μstrain with a standard deviation of 228 μstrain.

To get the high voltage into the packs, a flexible circuit is inserted in the blade assembly and runs along the blade web. A total of six plies of such circuits were designed, each of which has 8 copper leads inside a kapton insulation. All Flex Inc., Northfield, Minnesota manufactured the flexible circuits according to the specifications. They were successfully tested for high voltage isolation prior to the blade construction. Once the flex circuits are in place, their square-colder pads are soldered to the flaps (connectors) on the AFC packs, and each individual circuit layer is attached together and to the web using film adhesive cured at 250°F.

Finally, the fabrication of the Rohacell foam core inserts and the tantalum ballast weights for the leading edge and web. The Rohacell foam blocks were machined at NASA Langley's Advanced Machining Development Laboratory to the desired airfoil section, with an extra 10~15 mil oversize to ensure the right back compression of the laminate against the mold walls during cure. The foam blocks for the fairing were hand cut and sanded using a metal guide tool. The ballast weights were also fabricated at NASA Langley. The leading edge weights were machined to the desired shape, and the web ones were cut as small plate-like pieces.

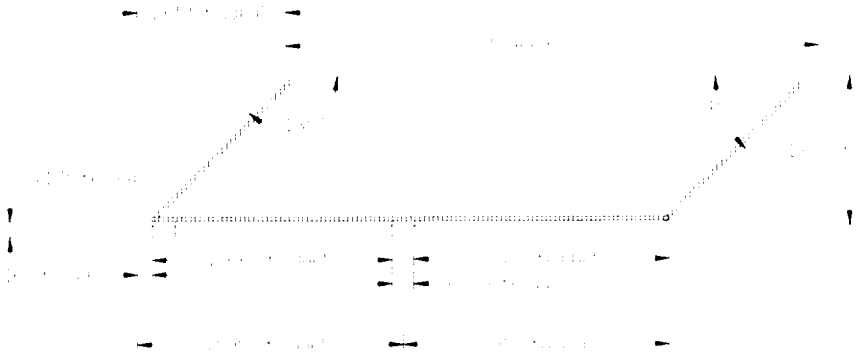

Figure 10. Final AFC pack design used in the ATR prototype blade

Testing Articles

Two testing articles were constructed prior to the final active prototype blade: a 1/3-span blade spar and a half-span blade spar (no-working AFC packs were used). Both are built with an aluminum attachment at the tip for gripping at the tensile testing machine. The first one was used primarily to debug the manufacturing process, including mold handling and usage, autoclave curing cycle (250°F, 90 min.—85 psi pressure was also used to support final closing of the mold), sliding of AFC packs in the prepreg laminate, the survivability of the AFC contact flaps through the curing cycle, the root construction, the Rohacell foam sizing and placement, and the attachment of strain gages on those foam pieces. The second testing blade was used primarily for testing the root strength and implementing modifications needed to the process identified from the first attempt. The improved manufacturing technique details used on the second blade checked all the steps to be followed on the full active blade.

After the tensile test, the second spar assembly was sliced to see any delamination of the plies or any voids trapped inside the assembly near the strain gages, and none was found. Also the weight of the spars was measured and compared with the target weight per unit length. Similarly, experiments were conducted to assess the spar torsional stiffness. Finally the fairing assembly of the same span length was attached and cured to the second spar successfully.

Prototype Blade

Now that the whole manufacturing process is well established, the fabrication of the ATR prototype blade followed.

Before starting the wrapping of the prepreg plies around the foam, sensors need to be properly installed and tested. A total of 10 sets of full-bridge strain gauge sensors are embedded into the foam core surface and the wires run through the small trough along the web. The 10 bridges are divided in six torsional strain gauges, three flap-bending strain gauges, all located at different spanwise stations, and one chordwise-bending strain gauge near the blade root. These strain gauges will be used to monitor the deformation and load level during spinning on the hover stand or in the wind tunnel. They are also helpful for individual pack actuation during bench tests.

The manufacturing of the spar assembly is conducted next. Two types of tantalum weight pieces are aligned and attached at the nose and rear web to give the desirable chordwise CG location and weight distribution. At the blade root, the stack of 80 graphite plies is inserted and at the discrete gap between the AFC packs and the root region is filled with S-Glass plies. The spar assembly is put inside the blade mold and sealed so vacuum can be built in the mold when inside the autoclave. The whole assembly in put inside MIT's autoclave and cured according to the cycle recommended by the prepreg manufacture.

Once the spar is cured, the six flex circuit layers are soldered to the corresponding AFC flap connectors using high-temperature solder. They are then bonded to each other and to the web using strips of film adhesive. Since the selected film adhesive was to be cured at 250°F, the spar plus flex circuit assembly was put in an oven for 90 minutes. Due to the mismatch of thermal expansion coefficients between the flex circuit (mostly composed of copper) and the composite spar assembly, an undesirable chordwise bending deflection resulted. This small deflection was significantly reduced once the fairing was attached and cured to the spar. The final shape of the ATR prototype can be seen in Fig. 11, and no major consequences are expected from the slight curvature present in the chordwise direction. The future wind tunnel blades will use a room temperature epoxy for the attachment of the flex-circuit layers to avoid this problem.

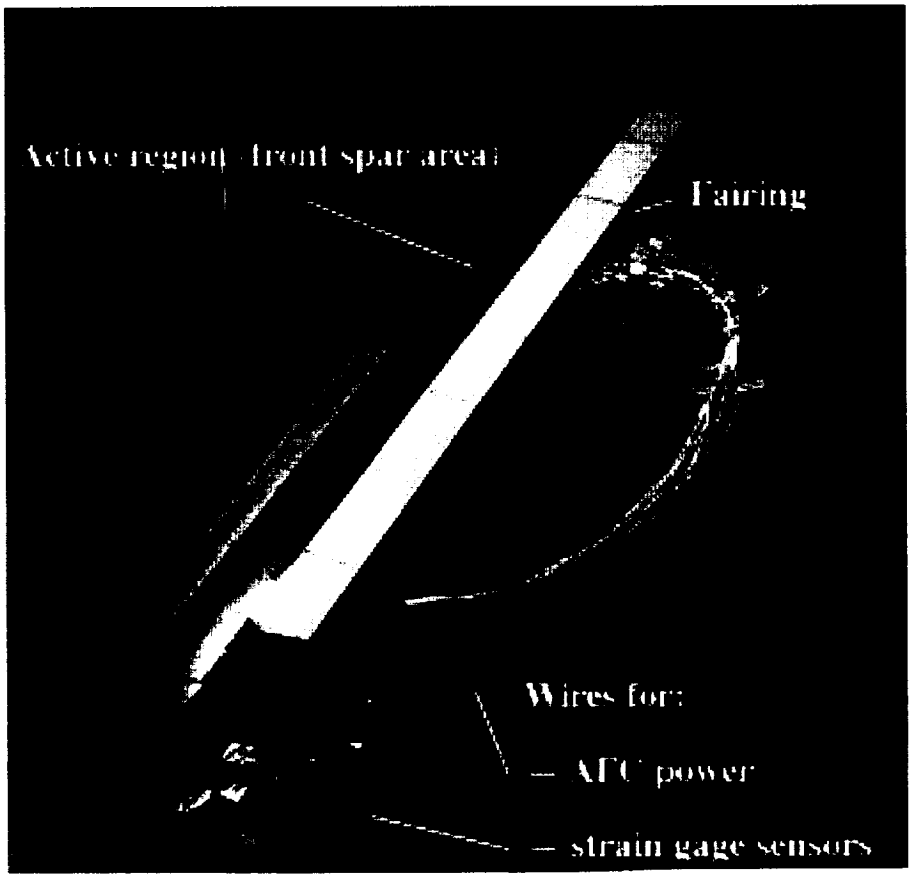

Figure 11. Final ATR prototype blade.

ATR PROTOTYPE RESULTS

In what follows, different characterization tests were performed on the ATR prototype blade in order to validate the design and manufacturing procedures, and to verify the performance of the prototype article.

Blade Root Test

As mentioned in the previous section, the second test spar was used for tensile testing of simulated centrifugal loads. This would primarily validate the root strength of the prototype blade.

From the blade design phase, estimates of the laminate ply strains at critical sections were performed based on the final assembly (spar and fairing). Those estimates combine the centrifugal loads resulting from the rotation of the blade at maximum nominal speed (687.5 rpm) and the worst forward flight aerodynamic loading (coming from CAMRAD II). Based on this information, an equivalent tensile load is calculated so to reproduce the worst case strain condition at the critical sections. Theoretical values based on maximum strain/first-ply failure criteria are calculated on the developed framework, and the results are presented in Table 3 for three critical blade section (BS) locations.

Table 3. Tensile load test on 3/4-radius blade spar (blade station in inches)

Critical Section Location	Tensile Load (N)
BS 6.87 (root inboard end)	4,608[1]
BS 12.5 (root transition region)	3,848[1]
BS 15.0 (root outboard end)	3,234[1]
Experimental Failure Load (> BS 15)	7,082[2]

[1] Calculated equivalent tensile load for first-ply failure/maximum strain criterion based on a full blade assembly (spar + fairing); CF load (687.5 rpm) + worst forward flight aerodynamic loading.
[2] Measured catastrophic failure load.

The half-span spar is assembled in the Instron machine so that the root is attached through three bolts to a metal assembly simulating the hub attachment, and the tip has a metal insert that is gripped directly to the moving head of the machine. Load was applied on increments of 100 lbf (444.8 N) up to 1,000 lbf, and then on increments of 50 lbf up to catastrophic failure. The spar broke at the uniform active cross-section region, at the middle of a bank of AFC packs. The fractured region was nearly perpendicular to the applied tensile load direction (see Fig. 12). The registered maximum tensile load was 1592 lbf (7,082 N), a factor of 1.54 higher than the worst case condition at the root and 1.47 higher than the worst design case condition for the active region. This result exceeds the NASA Langley Handbook wind tunnel model requirement of 1.25 factor of safety with respect to centrifugal loads.[27]

Figure 12. Testing article showing catastrophic failure under tensile loading.

Blade Torsional Stiffness Test

Since the blade torsional stiffness is an important parameter associated with the actuation authority of the blade, special attention is given to it. Tests were performed on the prototype blade before and after the fairing is attached. The tests were conducted on a specially built rig that applied a controlled couple at the tip of the blade, which stands vertically and is clamped at the root. A pair of laser sensors (Keyence LB-12, 2 μm resolution, 30~50 mm effective distance) was used to extract the rotation of a given station of the blade. Measurements were performed at different (active) stations at known radius separations, and at constant cross-sectional characteristics, for different levels of applied torque at the tip. A summary of the results in presented in Fig. 13, where the predicted results based on the developed thin-walled cross-sectional analysis and the more generic finite-element based VABS[20] are presented. As one can see, there is a significant increase (over 17%) on the blade torsional stiffness with the addition of the fairing. There is a considerably good overall correlation considering that the experimental data has a spread of approximately ±2 N-m^2 for the spar measurements and ±4 N-m^2 for the complete blade (difficulties were found on the load attachment device at the tip of the blade). The thin-walled approximation consistently under-predicts the torsional stiffness by 20%. Some of that is due to the model not accounting for the foam core, ballast weights, and the presence of the flexible circuit. A more detailed asymptotical modeling (VABS) based on a finite element discretization of the warping field, and including the effects of the foam core, shows a very good correlation with the experimental data.

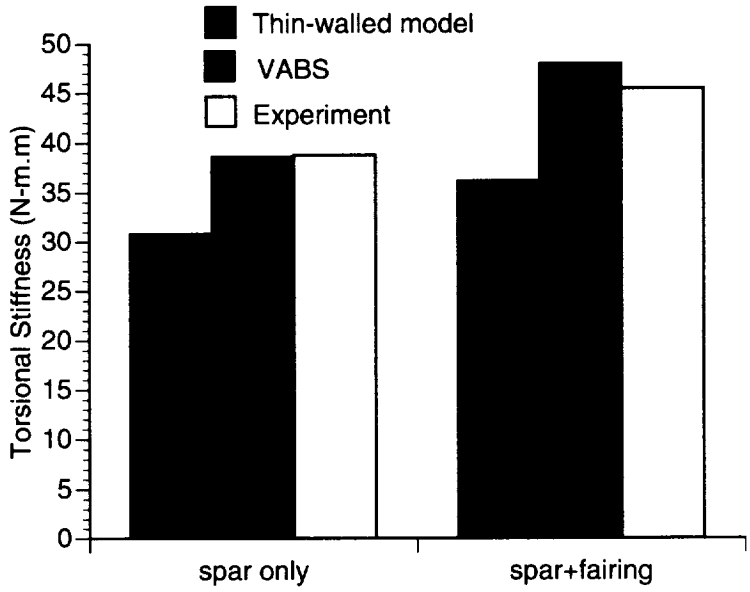

Figure 13. Torsional stiffness results for the spar and full blade–comparison between experimental and theoretical results

Bench Actuation Test

With the prototype blade mounted on the same rig as used for the stiffness tests, power was applied to the packs and a pair of laser sensors was used to measure the rotation angle at the tip of the blade. The amplifier used in these tests was a TREK 663A, ±10 kV, 20 mA, 40 kHz limiting current and frequency, respectively. These tests were performed on the spar first, and then on the whole assemble (spar + fairing).

The voltage was varied on increments of 500 V_{pp}, and the signal frequency was 1 Hz and 10 Hz for each voltage level (higher frequency tests were not possible with the given amplifier due to the current limitation). For voltages above 2,000 V_{pp}, a DC offset is used to avoid depolarization of the piezoelectric fibers. For 4,000 V_{pp} the scheduled DC offset is 800 V. During tests, however, AFC packs started short-circuiting once the voltage amplitude crossed 1,500 V. A total of five AFC packs short-circuited during the spar tests, while trying to establish the 2,000 V_{pp}/800 V_{DC} (the very first attempt to raise the voltage from 2,000 V_{pp}/0 V_{DC} to the 3,000 V_{pp}/800 V_{DC} was responsible for the first loss. All others happened at the 1,500 V_{pp}/800 V_{DC} and 2,000 V_{pp}/800 V_{DC}). Due to scheduled hover tests of this prototype blade, a decision was made to limit the maximum voltage applied at that point. All the packs lost in

these tests were on the same side of the blade, one per station from the inboard to one before the tip, and one being in the outer layer and all the others in the inner layer of AFC packs. No specific correlation among the failed packs was observed besides the voltage level. Similar problems were reported in Ref. 17, but all the attributed causes were eliminated from the present prototype blade. Further investigation on this issue is under way and finding will be reported in a later paper.

Table 4—Twist actuation of the ATR prototype blade (°/m, 2,000 V_{pp}/0 V_{DC})*

	Thin-Walled Model	Experiment
Spar only	2.0	1.1
Spar+fairing	1.8	1.0

* maximum measured twist was 1.5°/m at 2,000 V_{pp}/0 V_{DC} before any pack was lost.

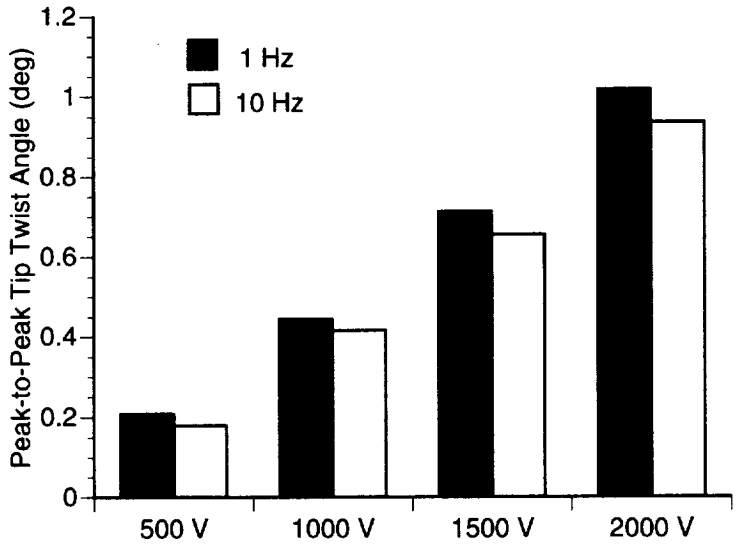

Figure 14. Actuation results of the ATR prototype blade having only 19 out of the 24 AFC packs working (voltage levels are peak-to-peak, no DC offset).

With 19 out of the original 24 AFC packs working, a summary of the voltage tests is presented in Fig. 14 for 1 Hz and 10 Hz excitation signals. As one can see from that plot, the 10 Hz response is consistently lower than the corresponding 1Hz one. This was expected based on a lower free strain response of the AFC packs with higher excitation frequency. Table 4 presents the twist rate for the spar alone and for the complete blade obtained from experimental measurements and from the model predictions (taking into account the five failed packs). The addition of the fairing had a small effect on the measured actuation level (~10% decrease), which indicates that the additional torsional stiffness (~17%) that comes along with the inclusion of the fairing is compensated by an increase in the block actuation moment. The change in the initial chordwise curvature is expected to have very small effect to the final actuation levels. As one can also see, the model overpredicted the actuation levels by a significant margin. Most of it can be associated with the fact that the predictions are based on linearized piezoelectric constants experimentally obtained at high fields (when 4,000 V_{pp} is used). The known nonlinear piezoelectric response as function of the electric field results in a lower effective d_{11} then the value reported in Table A.1. Other contribution to this error was already identified when predicting the torsional stiffness. Since the active twist rate is directly related to the torsional warping, similar problem found for the stiffness is reflected here (for example, the effects of the foam core that are neglected in the analysis). VABS is being upgraded to calculate the actuation strain constants,

and will be a more realistic analysis tool. It is worth noticing that the thin-walled multi-cell analysis formulation has been validated previously against other experiments,[21] showing a reasonably good correlation. The level of discrepancy here is way beyond previously found and may indicate that a potential AFC pack delamination from the composite laminate. No experimental evidence (other than the questioning above) has been found, and further non-destructive evaluation (NDE) tests will be performed. Finally, a typical twist actuation response for the ATR prototype blade is presented in Fig. 15.

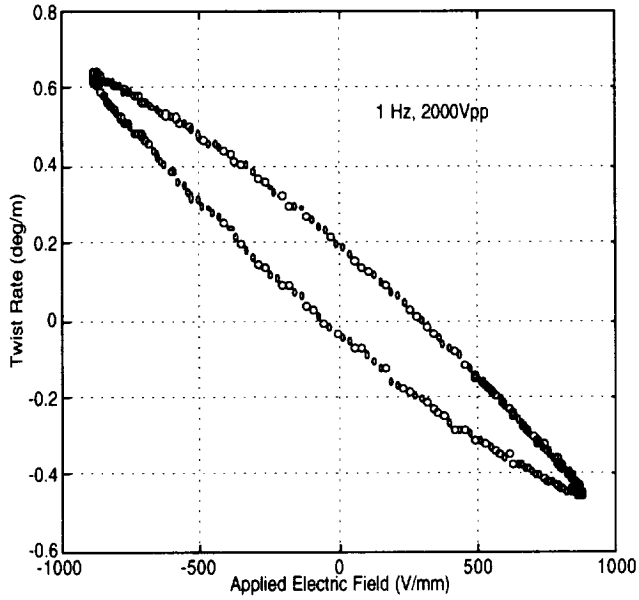

Figure 15. ATR prototype blade tip twist response as function of applied electric field (no DC offset).

CONCLUDING REMARKS

This work presents a main milestone on the joint program between NASA Langley/Army Research Laboratory and MIT on the study of helicopter hub vibration and noise reductions using the Active Twist Rotor system: the development of the prototype ATR blade. The presented modeling, design, manufacturing, and preliminary bench test results on this prototype blade will serve as the basis for further development of the desired aeroelastic research system composed of a four-bladed fully articulated rotor for wind tunnel tests, with each blade being integrally twisted by direct strain actuation. This is accomplished by distributing embedded piezoelectric active fiber composites along the span of the blades.

Experimental structural characteristics of the prototype blade compare well with design goals, and modeling predictions correlate fairly with experimental results. Preliminary bench actuation tests show lower twist performance than originally expected, and are due to electric failure of the active fiber composite actuators at high electric fields. A maximum twist of 1.5°/m (peak-to-peak) was reached at half of the operating voltage while all the actuators were working. The electric breakdown of the actuators is under intensive investigation at MIT and more tests need to be conducted on specially designed active coupons to narrow down the causes of failure under these circumstances.

Even with partial actuation capabilities, the prototype shows a significant achievement towards the construction of the full rotor system. The developed prototype blade will still be subject to a series of hover tests for further validation of its dynamic properties.

REFERENCES

1. Loewy, R. G., "Recent Developments in Smart Structures with Aeronautical Applications," Proceedings of the 37th Israel Annual Conference on Aerospace Sciences, February 26–27, 1997.

2. Friedmann, P. P., "The Promise of Adaptive Materials for Alleviating Aeroelastic Problems and Some Concerns," Proceedings of Innovation in Rotorcraft Technology, Royal Aeronautical Society, London, United Kingdom, June 24–25, 1997.

3. Spangler, R. L., Jr. and Hall, S. R., "Piezoelectric Actuators for Helicopter Rotor Control," Proceedings of the 31st AIAA/ASME/ AHS Structures, Structural Dynamics, and Materials Conference, Apr. 2-4, 1990, Technical Papers, AIAA Paper No. 90-1076, 1990, pp. 1589-1599.

4. Hall, S. R. and Prechtl, E. F., "Preliminary Testing of a Mach–Scaled Active Rotorblade with a Trailing Edge Servo–Flap," SPIE Smart Structures and Integrated Systems Symposium, Newport Beach, California, March 1, 1999.

5. Samak, D. and Chopra, I., "A Feasibility Study to Build a Smart Rotor: Trailing Edge Flap Actuation," SPIE Smart Structures and Materials Conference, Feb. 1-4 1993, Smart Structures and Intelligent Systems, Proceedings, Vol. 1917, Part 1, 1993, pp. 225-237.

6. Straub, F., "A Feasibility Study of Using Smart Materials for Rotor Control," Proceedings of the American Helicopter Society 49th Annual Forum, St. Louis, Missouri, May 1993.

7. Millot, T. and Friedmann, P., "Vibration Reduction in Helicopter Rotors Using an Actively Controlled Partial Span Trailing Edge Flap Located on the Blade," NASA Contractor Report 4611, June 1994.

8. Giurgiutiu, V., Chaudhry, Z., Rogers, C., "Engineering Feasibility of Induced Strain Actuators for Rotor Blade Active Vibration Control," Journal of Intelligent Material Systems and Structures, Vol. 6, No. 5, September 1995, pp. 583-597.

9. Fulton, M. V. and Ormiston, R., "Hover Testing of a Small-Scale Rotor with On-Blade Elevons," Proceedings of the American Helicopter Society 53rd Annual Forum, Virginia Beach, VA, April 29-May 1, 1997.

10. Barrett, R., "Intelligent Rotor Blade Structures Development Using Directionally Attached Piezoelectric Crystals," M.S. thesis, University of Maryland, College Park, MD, 1990.

11. Chen, P. and Chopra, I., "A Feasibility Study to Build a Smart Rotor: Induced Strain Actuation of Airfoil Twisting Using Piezoceramic Crystals," SPIE Smart Structures and Materials Conference, Feb. 1–4 1993, Smart Structures and Intelligent Systems, Proceedings, Vol. 1917, Part 1, 1993, pp. 238–254.

12. Derham, R. and Hagood, N., "Rotor Design Using Smart Materials to Actively Twist Blades," Proceedings of the American Helicopter Society 52nd Annual Forum, Vol. 2, Washington, D.C., June 4–6, 1996, pp. 1242-1252.

13. Wilkie, W. K., Belvin, W. K., and Park, K. C., "Aeroelastic Analysis of Helicopter Rotor Blades Incorporating Anisotropic Piezoelectric Twist Actuation," in ASME 1996 World Congress and Exposition, Adaptive Structures Symposium, Proceedings, Aerospace Division, November 1996.

14. Wilkie, W. K., Park., K. C., and Belvin, W. K., "Helicopter Dynamic Stall Suppression Using Active Fiber Composite Rotor Blades," AIAA Paper No. 98-2002, Proceedings of the 39th AIAA/ASME/AHS Structures, Structural Dynamics, and Materials Conference, Long Beach, California, April 20–23, 1998.

15. Rodgers, J. P., Hagood, N. W., and Weems, Douglas A., "Design and Manufacture of an Integral Twist-Actuated Rotor Blade," AIAA Paper No. 97-1264, Proceeding of the 38th AIAA/ASME/AHS Adaptive Structures Forum, Kissimmee, Florida, 1997.

16. Rodgers, J. P. and Hagood, N. W., "Preliminary Mach-Scale Hover Testing of an Integral Twist-Actuated Rotor Blade," presented at SPIE's 5th Annual International Symposium on Smart Structures and Materials, San Diego, California, March 1998.

17. Rodgers, J. P. and Hagood, N. W., "Development of an Integral Twist-Actuated Rotor Blade for Individual Blade Control," AMSL Report #98-6, Active Materials and Structures Laboratory, Massachusetts Institute of Technology, October 1998.

18. Bent, A., Hagood, N., and Rodgers, J., "Anisotropic Actuation with Piezoelectric Fiber Composites," Journal of Intelligent Material Systems and Structures, Vol. 6, May 1995, pp. 338–349.

19. Yeager, W., Mirick, P., Hamouda, M-N., Wilbur, M., Singleton, J., and Wilkie, W. K., "Rotorcraft Aeroelastic Testing in the Langley Transonic Dynamics Tunnel," Journal of the American Helicopter Society, Vol. 38, No. 3, July 1993, pp.73–82.

20. Cesnik, C. E. S. and Hodges, D. H., "VABS: A New Concept for Composite Rotor Blade Cross-Sectional Modeling," Journal of the American Helicopter Society, Vol. 42, No. 1, 1997, pp. 27–38.

21. Cesnik, C. E. S. and Shin, S. J., "Structural Analysis for Designing Rotor Blades with Integral Actuators," Proceedings of the 39th AIAA/ASME/AHS Structures, Structural Dynamics, and Materials Conference, Long Beach, CA, April 20–23, 1998, AIAA Paper No. 98–2107.

22. Hodges, D. H., "A Mixed Variational Formulation Based on Exact Intrinsic Equations for Dynamics of Moving Beams," International Journal of Solids and Structures, Vol. 26, No. 11, 1990, pp. 1253–1273.

23. Shang, X. and Hodges, D. H., "Aeroelastic Stability of Composite Rotor Blades in Hover," Proceedings of the 36th AIAA/ASME/AHS Structures, Structural Dynamics, and Materials Conference, New Orleans, Louisiana, April 10–12, 1995.

24. Johnson, W., CAMRAD II, Comprehensive Analytical Model of Rotorcraft Aerodynamics and Dynamics, Johnson Aeronautics, Palo Alto, California, 1994.

25. Wilkie, W. K., Wilbur, M. L., Mirick, P. H., Cesnik, C. E. S., and Shin, S.-J., "Aeroelastic Analysis of the NASA/ARMY/MIT Active Twist Rotor," Proceedings of the American Helicopter Society 55th Annual Forum, Montréal, Canada., May 25–27, 1999.

26. Cesnik, C. E. S. and Shin, S. J., "On the Twist Performance of a Multiple-Cell Active Helicopter Blade," Proceedings of the 9th International Conference on Adaptive Structures and Technologies, Cambridge, Massachusetts, 14–18 October 1998.

27. "Wind-Tunnel Model System Criteria," LHB 1710.15, NASA Langley Research Center, May 1992.

APPENDIX—Properties of the materials used on the fabrication of the ATR prototype blade

The following two tables present the material properties of the structural constituents of the ATR prototype blade.

Table A.1—Properties of the AFC packs.

Thickness	315 μm
Density	4,060 kg/m3
d_{11}^*	309 pm/V
d_{12}^*	−129 pm/V
Q_{11}	33.6 GPa
Q_{12}	7.54 GPa
Q_{22}	16.6 GPa
Q_{66}	5.13 GPa

* based on high-field linearization.

Table A.2—Properties of the composite materials used in the ATR prototype blade

	E-Glass	S-Glass	Graphite IM7 (root)
Resin	F-155	SP381	SP381
Weave	Fabric	Uni-tape	Uni-tape
Thickness (mm)	0.120	0.225	0.138
Density (kg/m3)	1700	1850	1550
E_{11}(GPa)	20.7	46.9	16.5
E_{22}(GPa)	20.7	12.1	8.83
ν_{-12}	0.13	0.28	0.34
G_{12}(GPa)	4.1	3.6	4.9

ACTIVE MATERIALS & STRUCTURES LABORATORY

DEPARTMENT OF
AERONAUTICS AND ASTRONAUTICS

Nesbitt W. Hagood IV
Associate Professor
of Aeronautics and Astronautics

ROOM 37-327
CAMBRIDGE, MASSACHUSETTS 02139
(617) 253-2738 FAX (617) 258-8336

December 3, 1999

NASA Center for Aerospace Information
Attn: Accessioning Department
800 Elkridge Landing Road
Linthicum Heights, MD 21090-2934

To Whom It May Concern:

Please find enclosed the End of fiscal Year letter for NASA Langley Research Center Contract # NCCI-259, for the proposal entitled "Development of an Active Twist Rotor for Wind-Tunnel Testing(NLPN 97-310).

If you have any questions or need further information, please do not hesitate to contact me at 617-253-2738

Sincerely,

Nesbitt W. Hagood IV

Enclosure (1)

Massachusetts Institute of Technology
77 Massachusetts Avenue
Room 37-315
Cambridge MA 02139-4307
tel 617-252-1536
fax 617-258-8336
http://web.mit.edu/amsl/